Article:
Jackson, LS and Forster, PM (2010) An Empirical Study of Geographic and Seasonal Variations in Diurnal Temperature Range. Journal of Climate, 23 (12). 3205 - 3221 . ISSN 0894-8755

https://doi.org/10.1175/2010JCLI3215.1

An Empirical Study of Geographic and Seasonal Variations in Diurnal Temperature Range

LAWRENCE S. JACKSON AND PIERS M. FORSTER

School of Earth and Environment, University of Leeds, Leeds, United Kingdom

(Manuscript received 21 April 2009, in final form 23 December 2009)

ABSTRACT

The diurnal temperature range (DTR) of surface air over land varies geographically and seasonally. The authors have investigated these variations using generalized additive models (GAMs), a nonlinear regression methodology. With DTR as the response variable, meteorological and land surface parameters were treated as explanatory variables. Regression curves related the deviation of DTR from its mean value to values of the meteorological and land surface variables. Cloud cover, soil moisture, distance inland, solar radiation, and elevation were combined as explanatory variables in an ensemble of 84 GAM models that used data grouped into seven vegetation types and 12 months. The ensemble explained 80% of the geographical and seasonal variation in DTR. Vegetation type and cloud cover exhibited the strongest relationships with DTR. Shortwave radiation, distance inland, and elevation were positively correlated with DTR, whereas cloud cover and soil moisture were negatively correlated. A separate analysis of the surface energy budget showed that changes in net longwave radiation represented the effects of solar and hydrological variation on DTR. It is found that vegetation and its associated climate is important for DTR variation in addition to the climatic influence of cloud cover, soil moisture, and solar radiation. It is also found that surface net longwave radiation is a powerful diagnostic of DTR variation, explaining over 95% of the seasonal variation of DTR in tropical regions.

1. Introduction

Existing research has identified factors such as solar radiation and cloud cover as influential for diurnal temperature range (DTR) over the global land surface, but how comprehensively do they account for the observed seasonal and geographic variation? This study describes the seasonal and geographic variations in DTR using empirical regression relationships with a selection of key meteorological and surface parameters. The aim is to quantify the relationships they have with DTR, to rank their importance, and advance understanding of the physical processes using an analysis of the surface energy budget.

Differences in DTR between regions are driven by seasonal and meridional variations in insolation (Geerts 2003). DTR is also modulated by differences in meteorological and surface parameters that exert an asymmetric influence on daily maximum and minimum temperatures. Increases in cloud clover, particularly low clouds, reduce daytime solar radiation reaching the surface, cooling maximum temperatures, and in high-latitude winters they trap longwave radiation and warm nighttime minimum temperatures (Dai et al. 1999). In autumn the relationship between cloud cover and DTR in the Northern Hemisphere is particularly strong. In September–November, the highest correlation between cloud cover and DTR was found for the United States (Karl et al. 1993). The greatest reduction in DTR associated with cloud cover was also found in September–November in the United States and Eurasia (Dai et al. 1999).

Precipitation is inversely correlated with DTR at regional scales (Dai et al. 1997), and the strongest reductions in DTR during the period 1950–2004 have been found in dry regions with low precipitation (Zhou et al. 2009). Soil moisture, which is replenished by precipitation, also influences DTR. The change from wet to dry seasons in a Rondonian pasture (Brazil) showed DTR doubled as the soil dried, while mean temperatures remained largely unchanged (Betts 2004). Atmospheric water vapor closes the water budget linking soil moisture, clouds, and precipitation, and increased humidity has been associated with reduced DTR (Linacre 1992).

Corresponding author address: Lawrence S. Jackson, School of Earth and Environment, University of Leeds, Leeds, LS2 9JT, United Kingdom.
E-mail: eelsj@leeds.ac.uk

DOI: 10.1175/2010JCLI3215.1

Geerts (2003) concluded that afternoon relative humidity exhibited the strongest relationship with DTR using observations recorded in January and July for locations between 65°N and 65°S.

The advection of air masses can have a large effect on DTR, especially in Arctic regions where dominant solar variations are often not diurnal (Przybylak 2000). Linacre (1982) argued that strong winds reduce DTR. Heat is transported away from the surface during the day, reducing maximum temperatures, and the nocturnal boundary layer air is mixed with warmer air entrained from above, limiting the extent of any nocturnal temperature inversion. Aerosols, which scatter or absorb solar radiation and exert cloud related indirect effects, could also influence DTR (Hansen et al. 1995). Solar dimming due to aerosols may, in part, explain the decreasing trend in DTR over Europe during 1950–85 (Wild et al. 2007). Weekly variations in the concentrations of aerosols [Bäumer et al. 2008 (Europe) and Murphy et al. 2008 (United States)] may also contribute to a ''weekend effect'' in DTR [Forster and Soloman 2003 (United States) and Gong et al. 2006 (China)].

In the 30–150-km range, DTR is greater the further inland one goes and this effect is more pronounced in the tropics than at higher latitudes (Geerts 2003). Sites beside large inland lakes or seas experience DTRs lower than other continental sites. In contrast, the relationship between DTR and elevation is not so straightforward. Linacre (1982), in a review using many mountain locations, concluded that there were widely differing relationships between DTR and elevation. Land use and land cover can cause significant variations in DTR through differences in surface albedo, evapotranspiration, and longwave (LW) radiation (Gallo et al. 1996). Changes in foliage and the growth of vegetation or crops can also add a seasonal dimension to DTR variation (Eastman et al. 2001).

Our study builds on these previous results using regression relationships to describe the climatology of DTR for the majority of the global land area. We investigate the relationship between monthly mean DTR and vegetation, meteorological, and energy budget parameters. The physical mechanisms controlling DTR are interpreted through analysis of regression curves and the surface energy budget (SEB). Section 2 describes the datasets used and section 3 describes our methods. Our results are presented in section 4. Section 4a describes the geographic variation in monthly mean DTR, section 4b describes results from single variable generalized additive models (GAMs) using meteorological and surface parameters as explanatory variables. Section 4c describes results from a multivariate GAM model and section 4d results from GAM and linear regression models using SEB terms as explanatory variables. Discussion of the results and conclusions follow in section 5.

2. Data

The analysis of seasonal and geographic variations in DTR was based on monthly mean data averaged over the years 1983–2002 or a shorter period when data were not available for the full 20 years (Table 1). The data for DTR, other meteorological, and land surface parameters were obtained from a variety of sources available in different formats (Table 1). These data were processed into 0.5° × 0.5° resolution gridded datasets based on Climatic Research Unit (CRU) TS 2.1 (Mitchell and Jones 2005) covering the global land area excluding Antarctica. We found that values of DTR recorded in CRU TS 2.1 over Greenland were periodically much greater than values reported by the Arctic studies of Tuomenvirta et al. (2000) and Ohmura (1984). Annual mean DTR in Greenland and its seasonal variation were also substantially larger than recorded elsewhere over land. Therefore data for Greenland were removed by excluding grid boxes north of 60°N and bounded between 60°W and 0° longitude. The monthly mean data were averaged over all years, giving 12 values for each of the remaining 0.5° × 0.5° grid boxes, one for each month. Data for monthly mean DTR were calculated from CRU TS 2.1 maximum and minimum temperature data. Data for monthly mean precipitation, cloud cover, and elevation were also taken from CRU TS 2.1 (Mitchell and Jones 2005).

Data from sources other than CRU TS 2.1 were not always available over the same time period or at the same grid resolution. Data were selected to match as close as possible the 1983–2002 time period. For data only available at a lower resolution, point values from the larger grid were copied without change in value to the 0.5° × 0.5° CRU grid format. Only land data were employed from globally gridded datasets. Distance from the coast was estimated from the center of each CRU grid cell, using the CRU TS 2.1 land mask and assuming the earth to be a sphere with radius 6378 km.

The 40-yr European Centre for Medium-Range Weather Forecasts (ECMWF) Re-Analysis (ERA-40) (Uppala et al. 2005) was used for data on surface energy fluxes, cloud height, soil moisture, evaporative flux, wind speed, dewpoint temperature, and surface air temperature. ERA-40 data for cloud cover were only used to interpret our regression results and were not used in the development of the regression models. ERA-40 surface air temperature data were used to derive dewpoint depression and not for DTR. All DTR data were from CRU TS 2.1. Surface albedo was derived from ERA-40

TABLE 1. Sources of data used for explanatory variables in the regression analysis. Grid resolution is shown as longitude × latitude.

Description	Resolution	Time period	Source
CRU TS 2.1: monthly mean maximum and minimum temperatures, cloud cover, precipitation, vapor pressure, and gridcell elevation	0.5° × 0.5°	1983–2002	Mitchell and Jones (2005)
MISR level 3 global aerosol product (monthly) (http://eosweb.larc.nasa.gov/PRODOCS/misr/products/level3.html)	0.5° × 0.5°	2000–02	Langley Atmospheric Science Data Center (ASDC); Diner et al. (1998)
Monthly average TOA insolation derived with the Quality-Check SW (QCSW) algorithm of the National Aeronautics and Space Administration (NASA) World Climate Research Programme/Global Energy and Water Cycle Experiment (WCRP/GEWEX) Surface Radiation Budget (SRB) Project. Dataset: SRB REL2.5 QCSW MTHLY (http://eosweb.larc.nasa.gov/cgi-bin/searchTool.cgi?Dataset=SRB_REL2.5_QCSW_MONTHLY)	1° × 1°	1984–2002	Langley ASDC; Darnell et al. (1992)
Primary vegetation, secondary vegetation, and soil type	1° × 1°	Varies	Wilson and Henderson-Sellers (1985)
ERA-40 reanalysis data: cloud cover level (low–medium–high), soil moisture; surface shortwave and longwave radiation, latent heat, sensible heat, evaporation, wind speed, dewpoint temperature, and surface air temperature (http://www.ecmwf.int/research/era/do/get/era-40)	2.5° × 2.5°	1983–2001	ECMWF data (http://badc.nerc.ac.uk/data/ecmwf-e40/); Uppala et al. (2005)

data for net surface shortwave (SW) radiation and downward surface SW radiation. Bowen ratio was calculated from ERA-40 surface sensible and latent heat fluxes. Satellite data were used for aerosol optical depth (Diner et al. 1998) and top-of-atmosphere (TOA) SW radiation (Darnell et al. 1992). See Table 1 for details.

3. Methods

a. Single variable regression

Employing the monthly mean data in section 2, regression analysis was used to identify the parameters that had the strongest relationship with seasonal and geographic variation in DTR. The meteorological and land surface parameters were treated as explanatory variables. A separate regression was performed for each explanatory variable. Each model included one regression curve describing the relationship between deviation of DTR from its global annual mean value and values of the explanatory variable. The shape of the regression curve was helpful in interpreting the physical mechanisms by which the variables influence DTR. We define DTR deviance explained as the proportion of seasonal and geographic variation in DTR data that was explained by a regression model. The variations in DTR were measured relative to its mean value. Deviance explained was used as a measure of goodness of fit and also a measure of the strength of the relationship between DTR and each parameter. These results are shown in section 4b.

b. Multivariate model

The next stage was to develop a multivariate regression model to quantify the relative importance of the parameter relationships. The gridded dataset was divided into 84 subsets comprising combinations of seven vegetation groups and 12 months. A multivariate regression model was fitted individually to each of the 84 data subsets using a stepwise regression approach starting with no explanatory variables. The parameters were tested in the regression model one at a time and the parameter that yielded the largest increase in deviance explained was retained in the model. This process was repeated until adding further variables did not lead to an appreciable increase in deviance explained. To validate that variable selection was optimal, each variable in the final model was replaced in turn with alternatives to confirm that the fit to data deteriorated in each case. The results are shown in section 4c. Colinearity was tested for using the variance inflation factor for each explanatory variable. A maximum value of 5 was accepted (see Montgomery and Peck 2006 for details). If this value was exceeded, the collinear variable making the least contribution to deviance explained was removed from the regression model. Each variable was checked for a p value significant at the 0.1% level. In models that had a good fit to

DTR data the sensitivity of results to changes in parameters in the curve fitting process was checked. The residuals were inspected to confirm, first, that their distribution was approximately Gaussian with zero mean and second, that they exhibited no clear relationship with the explanatory variables or fitted values.

c. Surface energy budget

To aid interpretation of the physical processes by which the explanatory variables influence DTR, the relationships between monthly mean DTR and surface energy budget terms were investigated using regression analysis. The results are shown in section 4d. Each model included one regression curve describing the relationship between deviation of DTR from its global annual mean value and values of the explanatory variable. The explanatory variables were net surface SW and LW radiation, surface sensible heat, and surface latent heat fluxes. A separate regression relationship was developed for each explanatory variable because the strong correlations between surface energy budget terms would make interpretation of a multivariate regression difficult. It was also for this reason that energy budget and meteorological parameters were not combined in a multivariate model.

Geographic variation in the relationship between net LW radiation and DTR was investigated further using linear regression. DTR was treated as the response variable. The regression was applied separately in each grid cell using 12 monthly mean values for DTR and net LW radiation.

d. GAMs

GAMs (Hastie and Tibshirani 1990) were used for the nonlinear regression calculations. GAMs have proved useful for representing nonlinear meteorological relationships in investigations in to atmospheric pollution like, for example, nitrogen dioxide concentrations (Carslaw and Carslaw 2007), benzene, and 1,3-butadiene (Reiss 2006). GAMs have also been used to identify an association between increased DTR and increased acute mortality from respiratory and cardiovascular conditions in Shanghai, China (Kan 2007).

In the GAM regression, the relationship between DTR and the explanatory variables was described by a constant term and a separate regression curve for each explanatory variable. The constant term represented the mean DTR over the data subset used. The regression curves (Figs. 2, 6, and 7) represented how DTR varied away from this mean level (on the y axis) with values of the explanatory variable (on the x axis). The shape of each regression curve was interpreted qualitatively to gain insight into the relationship with DTR.

GAM regression curve fitting was performed using tensor product regression curves (Wood 2006), which were found to perform well with the large quantity of data employed. Thin plate regression splines were used when an increase in degrees of freedom improved the fit to the data. Each individual regression curve was fitted with between 4 and 9 degrees of freedom in both the single variable GAMs and the multivariate GAM. The statistical software R (version 2.5.0 for Windows; R Development Core Team 2007) was used for all calculations and the integrated mgcv package (version 1.3–23) was used to fit the regression curves.

Great care was exercised when interpreting the regression curves. Emphasis was placed on prominent features derived from large amounts of data that could be related to known physical processes. Spurious features in the regression curves could come from many sources including the lack of independence in explanatory variables, the influence of the tails of the curves where there is greater uncertainty, paucity in data over parts of the range of observed values, and small-scale peaks and troughs in curve shape from overfitting data. Just as importantly, variables not included in the regression analysis could have been responsible for the variation in DTR.

4. Results

a. Monthly mean DTR

Figure 1 shows the geographic pattern of monthly mean DTR for the months of January, April, July, and October. Tropical regions and particularly deserts had the highest DTR values and coastal areas had relatively low values that were presumably due to the influence of the marine environment. DTR had its smallest annual cycle in the equatorial rain forest regions and the Sahara Desert. This contrasted with the high latitudes where there was large seasonal variation in DTR.

b. Single variable regression

Monthly mean DTR was regressed against each parameter in turn and the deviance explained recorded as a measure of the strength of the relationship (Table 2). All regression models included a constant term equal to the global annual mean DTR (11.0°C). Deviations of DTR from this mean value are shown on the y axes of the regression curves. Large deviations from the mean DTR may indicate an influential relationship with DTR.

The monthly mean temperature less the dewpoint temperature (dewpoint depression, DPD) had the largest explained deviance (Table 2). The regression curve (Fig. 2a) shows greater DPD to be associated with greater DTR

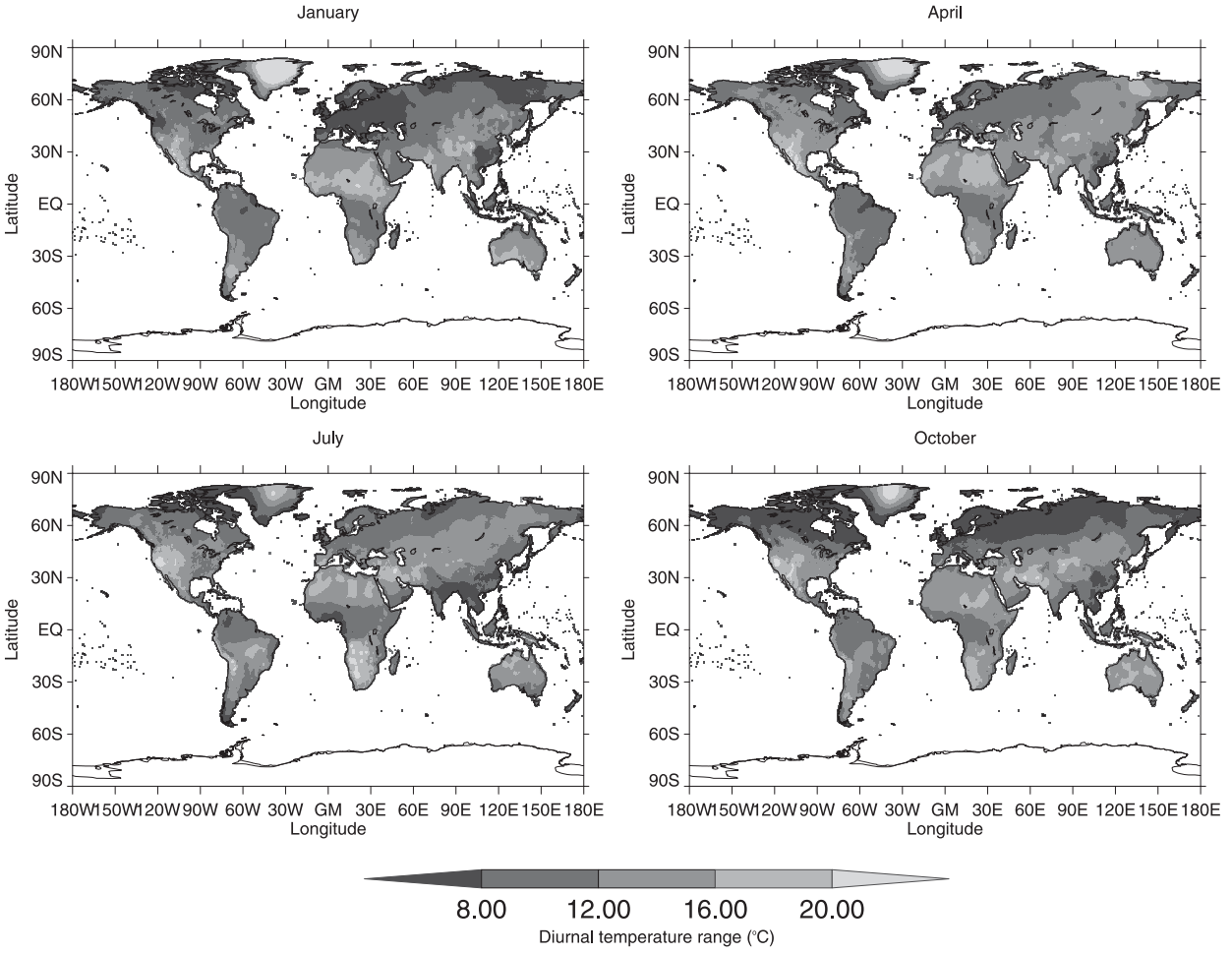

FIG. 1. Monthly mean DTR for January, April, July, and October. DTR data were from CRU TS 2.1 and averaged over the years 1983–2002.

consistent with Linacre (1992). However, it is a temperature parameter closely related to DTR and therefore does little to help understanding. Cloud cover, soil moisture, and distance inland were included in the multivariate GAM and are described in section 4c. The regression curve for latitude matches the mean latitudinal distribution of DTR (Fig. 2b). Twin maxima at 30°N and 30°S reflect the high DTR of the subtropical high pressure zones. Latitude was not used in the multivariate GAM because monthly mean downward TOA solar radiation provided a better fit to the seasonal variation in DTR. Vegetation group, elevation, and downward TOA solar radiation were included in the multivariate GAM and are described in section 4c. The regression curve for maximum temperature (not shown) showed larger maximum temperatures associated with larger DTR. Maximum temperature was not used in the multivariate GAM because of its high correlation with downward TOA solar radiation. The regression curve for albedo (Fig. 2c) showed larger albedo was associated with greater DTR up to an albedo of ~0.25. Beyond an albedo of 0.25, larger albedo was associated with smaller DTR.

Vapor pressure (Fig. 2d) explained only 14.3% of the variance in DTR. Above 15.0 hPa, greater vapor pressure was associated with smaller DTR, explained deviance improved to 33.1%, and vapor pressure was positively correlated with cloud cover (+0.50). Therefore, at these high vapor pressure levels humidity appears to be coupled with cloud cover in influencing DTR. Increasing precipitation was associated with decreasing DTR (Fig. 2e) although deviance explained was low (14.1%). Precipitation exhibited positive correlations with water vapor pressure (+0.63), surface evaporation (+0.63), and cloud cover (+0.45).

Aerosol optical depth (AOD) explained only 6.7% of the variation in DTR and the nature of the relationship is unclear (Fig. 2f). This weak relationship maybe genuine or because the effect of AOD is confounded

TABLE 2. Deviance explained, the proportion of the variation in DTR explained individually by each variable using a GAM model. The variation in DTR is the variation of monthly mean CRU gridcell values from the global annual mean DTR. These results are described in section 4b.

Variable name	Deviance explained (%)
Dewpoint depression	56.2
Percent cloud cover	42.2
Soil moisture	24.6
Distance inland	23.9
Latitude	23.8
Mean daily maximum temperature	21.9
Vegetation group	21.3
Elevation	19.8
Downward TOA SW radiation	18.9
Surface albedo	16.1
Vapor pressure	14.3
Precipitation	14.1
Aerosol optical depth	6.7
Evaporation	3.0
Longitude	2.2
Scalar wind speed	0.6

with other parameters and/or there are significant AOD measurement uncertainties associated with the Multiangle Imaging SpectroRadiometer (MISR) data (Diner et al. 1998). Evaporation, longitude, and scalar wind speed each accounted for 3% or less of the variation in DTR.

c. *Multivariate model*

Five explanatory variables were selected to maximize deviance explained: cloud cover, downward TOA SW radiation, distance inland, elevation, and soil moisture. As stated in section 2, the data were divided into 84 subsets comprising combinations of seven vegetation groups and 12 months. Regression models were fitted separately for each of the 84 subsets. Each regression model had a constant term representing the monthly mean DTR for the month and vegetation group in question and five regression curves with between 4 and 9 degrees of freedom each. The combined results are referred to as GAM_{dtr}.

All regression curves in GAM_{dtr} were significant at 0.1% except for the elevation curve during March for the inland water–bog–coastal-vegetation type. This regression curve was not significant, and removing it from the GAM had a negligible effect on the results. Combined results from the 84 models produced an unbiased estimate of the global annual mean DTR and deviance explained of 79.7% (80.3% for the Northern Hemisphere and 72.5% for the Southern Hemisphere). The largest errors in estimated monthly mean DTR were −0.1°C for the Northern Hemisphere and +0.4°C for the Southern Hemisphere with both maxima occurring in September. Deviance explained varied systematically by month and was greatest during October in the Northern Hemisphere (86.7%) and during June in the Southern Hemisphere (74.0%). The lowest deviance explained was found for April in the Northern Hemisphere (68.4%) and for March in the Southern Hemisphere (62.8%). Deviance explained was lowest for the inland water/bog/coastal vegetation type (68.2%) followed by vegetation types for grassland (70.7%), evergreen forest/wood (71.2%), mixed deciduous forest/wood (71.6%), semiarid and shrub (76.1%), and cropland (82.1%) and largest for barren land (87.6%).

To validate GAM_{dtr}, bootstrapping with a 50% sample of data was used to calibrate the GAM and predict values that could be compared against the remaining data. This process was repeated 100 times and the results shown in Fig. 3. The predicted mean DTR was unbiased at 11.5°C based on data points with complete data for the explanatory variables. The root mean squared error (RMSE) was 1.5°C. Predicted DTR values exceeded observations in central and southeastern China, the north of India, and the Arabian Peninsula. Predicted DTR values were less than observations in parts of the United States, Mexico, the Buenos Aires region of Argentina, and the Sakha region of Russia.

The five explanatory variables selected for GAM_{dtr} were not unique in producing a close fit to the DTR data. Replacing soil moisture with precipitation in GAM_{dtr}, while retaining the other four explanatory variables and the vegetation and month subdivisions, increased deviance explained by 0.3%–80.0%. Soil moisture was preferred over precipitation because its correlation with other explanatory variables was lower.

To assess the individual contributions of vegetation group, month, and the five explanatory variables toward explaining the variation in monthly mean DTR, each variable was removed in turn from GAM_{dtr} and the deviance explained recalculated (Table 3). The reduction from 5 to 4 explanatory variables or the reduction of data subsets from 84 to 7 (removing month) or to 12 (removing vegetation group) reduced deviance explained. The larger the reduction in deviance explained the greater the contribution made toward explaining the variation in monthly mean DTR. Vegetation made the greatest contribution. Cloud cover also ranked highly. The effect of adding a sixth regression curve to GAM_{dtr} was also tested and found to make little difference.

Figure 4 shows the geographic location of the seven vegetation types. Regions with high mean DTR values (e.g., shrub and semiarid) were typically in dry sunny climates where daytime insolation and limited evaporative cooling would be expected to contribute to the high DTR. Inland water/bog/coastal was found to have low DTR and damped seasonal variation. In these regions there is

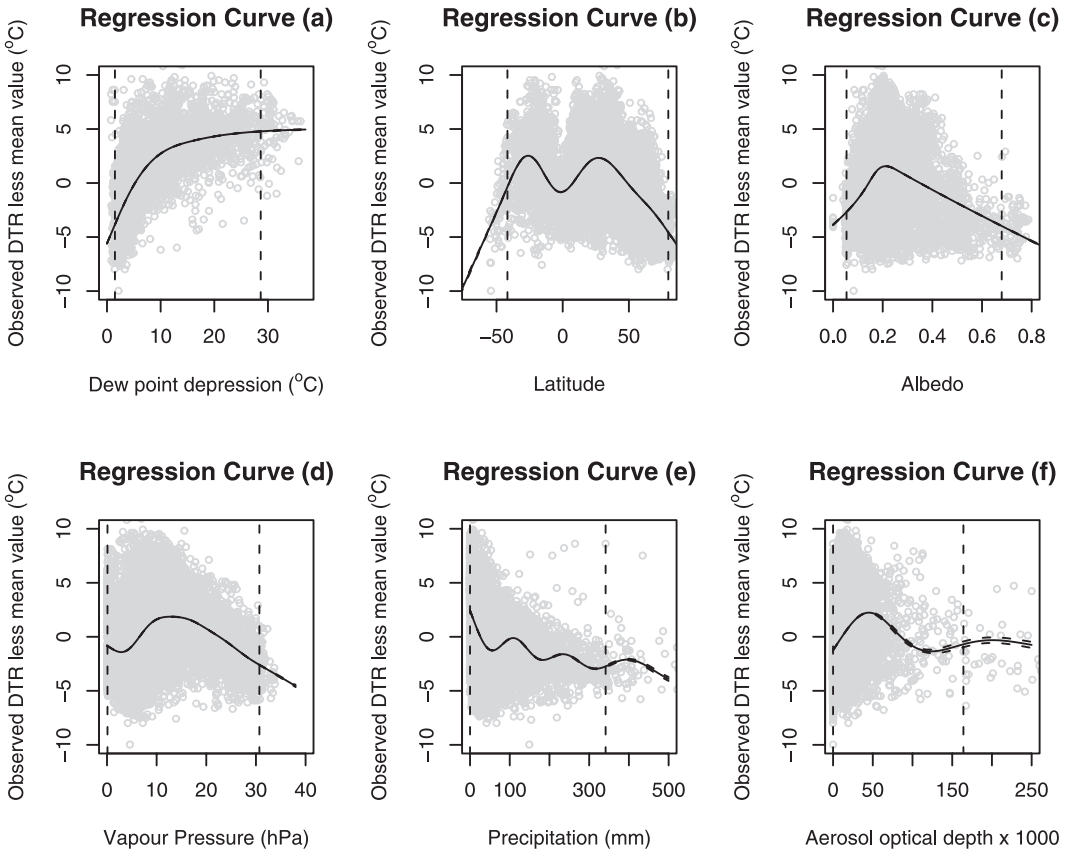

FIG. 2. Regression curves for (a) dewpoint depression (°C), (b) latitude (°), (c) surface albedo, (d) vapor pressure (hPa), (e) precipitation (mm), and (f) aerosol optical depth. Variation in DTR from its mean value is shown on the *y* axes. Variations in the explanatory variables are shown on the *x* axes. Confidence intervals at 95% are shown, although they are not clearly visible where they track the regression curves very closely. Two vertical dashed lines show the 1st and 99th data percentiles. Gray shading shows the distribution of a random sample of the underlying data.

plentiful surface water, which presumably cools maximum temperatures more than minimum temperatures because of daytime evaporation. The effect of grouping data by vegetation type in GAM_{dtr} was compared to randomized grouping; deviance explained reduced from 79.7% to 73.7% when randomized vegetation groups were used. The significance of vegetation was tested by rerunning GAM_{dtr} without vegetation groups. The residuals were grouped according to vegetation type and compared to a normal distribution with mean zero. A null hypothesis that the residuals were normally distributed was rejected at the 0.1% significance level for all seven vegetation types. Therefore, vegetation type, or its associated climatology, is strongly related to DTR even after important climatic parameters have been allowed for.

Seasonal variation in DTR is depicted in Fig. 5 with the largest DTRs in spring (April in the Northern Hemisphere and August in the Southern Hemisphere) and the smallest DTRs in autumn (November and March for the Northern and Southern Hemispheres, respectively). As expected seasonal variation in DTR is muted in coastal regions and the equatorial zone (Geerts 2003).

Each of the five explanatory variables in GAM_{dtr} has 84 regression curves. Figure 6 shows the mean regression curve for each explanatory variable and the 95% confidence intervals. The relative performance of each parameter in the overall model is described in the remainder of this section.

Greater cloud cover was strongly associated with smaller DTR in a relationship that was almost linear (Fig. 6a). Low-level clouds were more influential for DTR than higher-level clouds (Table 4). Generally, increased TOA solar radiation was associated with increased DTR (Fig. 6b). However, at solar radiation higher than ~350 W m^{-2}, DTR decreases and then increases again beyond solar radiation levels of 425 W m^{-2}. This dip is associated with equatorial grid points and is likely due to solar radiation having a smaller surface

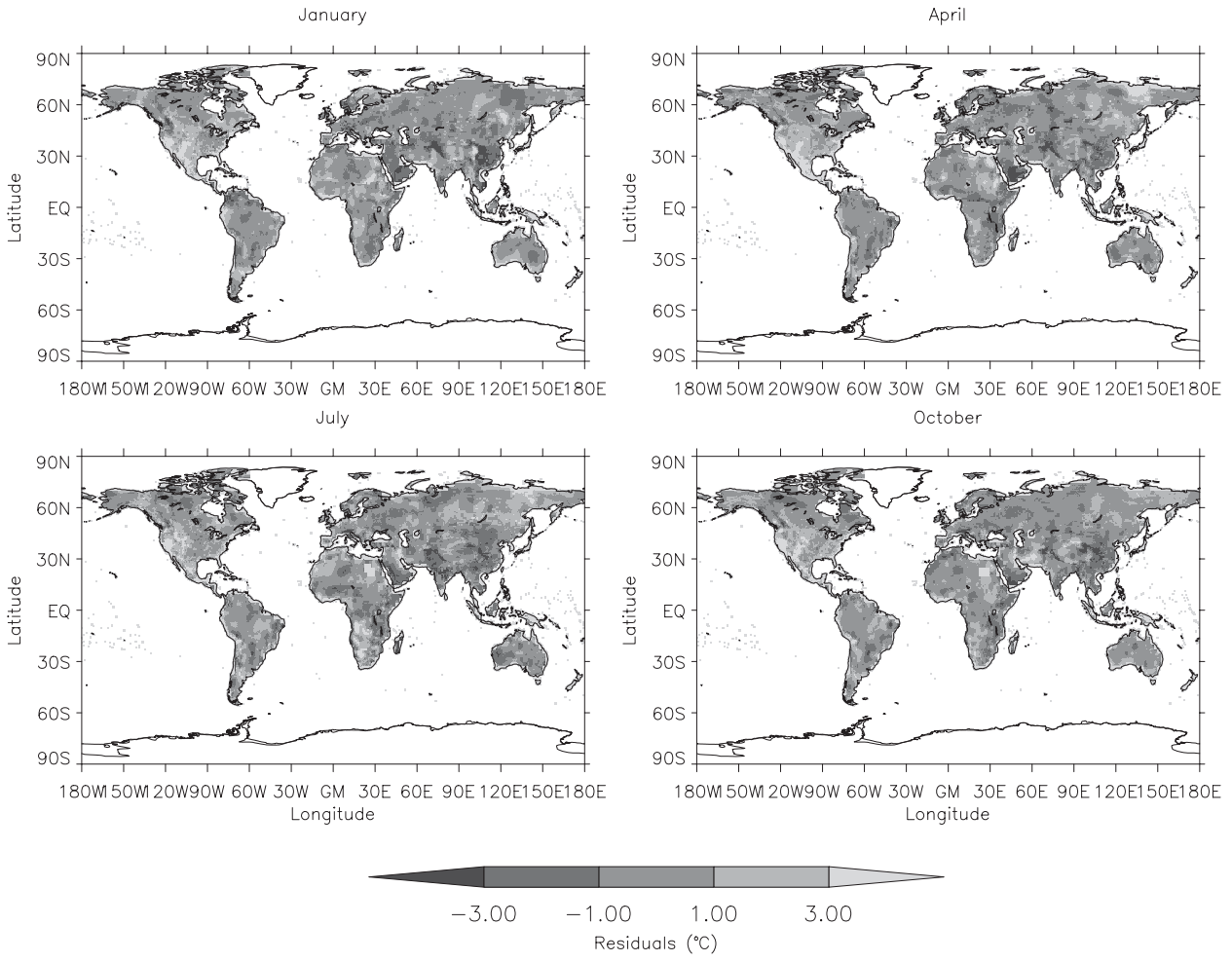

FIG. 3. Mean residuals (observed less predicted) from the prediction of DTR using 100 iterations of GAM_{dtr} using 50% of the data to calibrate the model and then predict the remaining 50% of the data: (top) (left) January and (right) April; (bottom) (left) July and (right) October.

influence because of attenuation by the deep, moist, and cloudy atmosphere. This result is supported by the regression curve for latitude (Fig. 2b), which has the same shape over each hemisphere.

Greater distance inland was associated with larger DTR (Fig. 6c). At distances larger than 2000 km the result may not be robust as there were progressively fewer data and local influences associated with continental Asia become increasingly dominant.

Larger elevations above sea level were associated with larger DTR (Fig. 6d). Elevation was partially correlated with distance inland (+0.36) and the correlation was particularly strong for China (+0.80). The correlation coefficients for other parameters, which may contribute to this elevation effect included water vapor pressure (−0.23), cloud cover (−0.14), and soil moisture (+0.03).

The regression curve between soil water volume and DTR showed no relationship from 0.0 to 0.2 m^{-3} $(m^{-3})^{-1}$ of soil moisture (Fig. 6e). Soil water volume of up to 0.2 m^{-3} $(m^{-3})^{-1}$ may be required to overcome resistance to evapotranspiration from stomata and the soil surface (Camillo and Gurney 1986). Above 0.2 m^{-3} $(m^{-3})^{-1}$ increases in soil moisture were associated with decreases in DTR. This might be expected because of increased daytime cooling from evapotranspiration, although the correlation of soil moisture and evaporative flux above the soil moisture level of 0.2 m^{-3} $(m^{-3})^{-1}$ was only +0.16.

d. Surface energy budget

Monthly mean DTR was regressed against each SEB component with data for vegetation types and months aggregated. Most terms in the SEB were highly correlated, rendering them unsuitable for multivariate analysis. Deviance explained is shown in Table 5 and regression curves in Fig. 7. All regression models included a constant term equal to the global annual mean DTR 11.0°C.

TABLE 3. Change in deviance explained by adding or removing individual variables from GAM_{dtr}. The deviance explained by GAM_{dtr} was 79.7%. The variation in DTR is the variation from the mean for each month and vegetation data subgroup. The results are described in section 4c.

	Change in deviance explained (%)
Removing	
Vegetation group	−6.5
Monthly grouping	−6.2
Cloud cover	−5.1
Distance inland	−4.1
Downward TOA SW radiation	−4.0
Elevation	−2.9
Soil moisture	−2.4
Adding	
Precipitation	2.2
Vapor pressure	2.2
Evaporation	0.9
Aerosol	0.5
Scalar wind	0.5

With respect to energy fluxes, a positive (negative) sign represents a flux toward (away from) the surface.

Net surface LW radiation was highly correlated with DTR (−0.74) with a greater flux away from the surface associated with greater DTR. This relationship was also reflected in the high deviance explained (57.3%), which improved (62.0%) when separate regression curves were used for upward and downward surface LW radiation. At fluxes less negative than −100 W m^{-2}, the regression curve (Fig. 7a) was approximately linear. At fluxes more negative than −100 W m^{-2}, the regression curve was roughly flat, indicating a break in the relationship with DTR. Using this GAM to estimate the observed seasonal and geographic pattern of DTR yielded an unbiased estimate with RMSE of 2.1°C. DTR was overestimated in January, April, July, and October in the southern part of the Arabian Peninsula, the Tamanrasset region of the Sahara Desert, and southeastern China. In the Sakha region of eastern Russia, DTR was overestimated in January while it was underestimated in April and July. Other regions where the model underestimated DTR included parts of the United States, Mexico, northern Angola, southern Peru, and the Himalayas.

Larger sensible heat fluxes from the surface were associated with larger DTR (Fig. 7b), and over commonly experienced flux values the relationship was broadly linear. At levels more negative than ~−80 W m^{-2}, greater sensible heat fluxes did not contribute to greater DTR.

The Bowen ratio is the ratio of sensible to latent heat flux (Bowen 1926). It was found to have a similar deviance explained as sensible heat flux (Table 5). Less than a Bowen ratio of zero, the data are from mid- to high-latitude locations mainly for the winter, spring, and summer seasons. Between a Bowen ratio of zero and four, DTR has a broadly linear relationship with Bowen ratio, with larger ratios associated with greater DTR

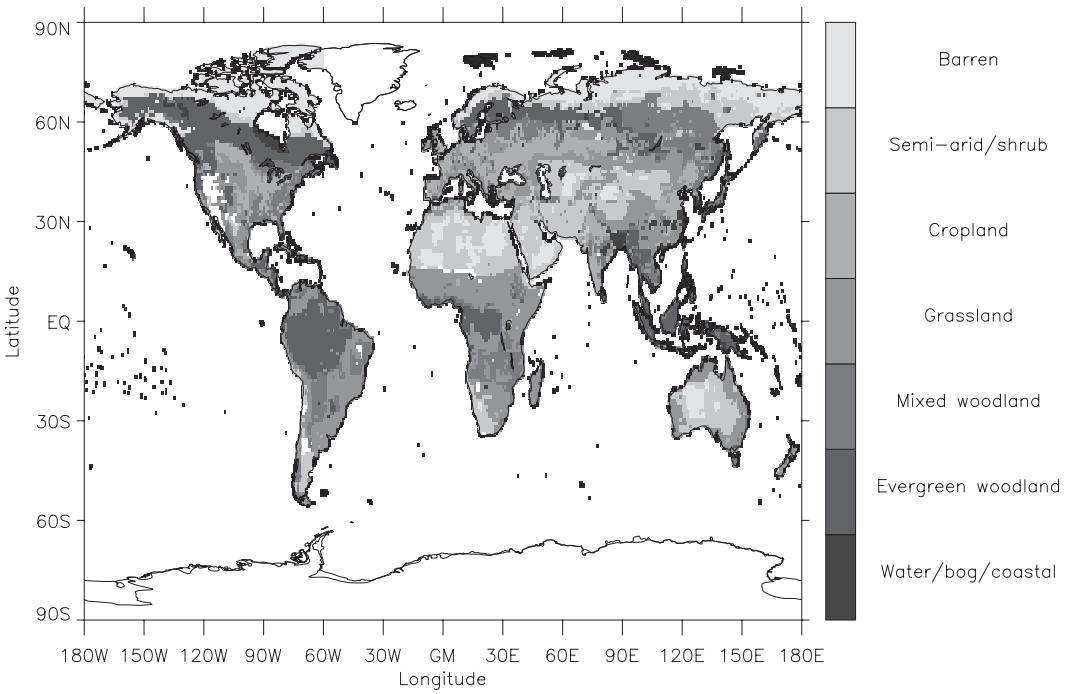

FIG. 4. Geographic distribution of the seven vegetation groups.

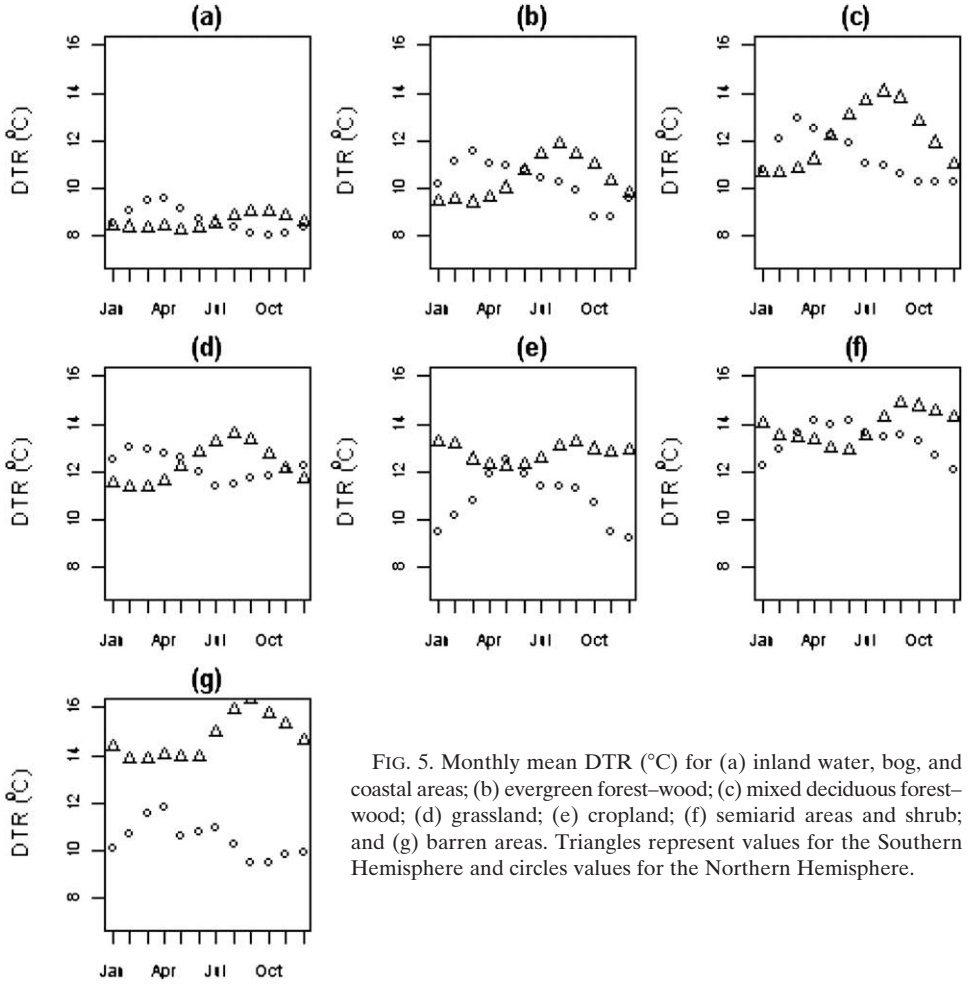

FIG. 5. Monthly mean DTR (°C) for (a) inland water, bog, and coastal areas; (b) evergreen forest–wood; (c) mixed deciduous forest–wood; (d) grassland; (e) cropland; (f) semiarid areas and shrub; and (g) barren areas. Triangles represent values for the Southern Hemisphere and circles values for the Northern Hemisphere.

(Fig. 7c). However, the deviance explained over this range (34.2%) is less than over the full range of data, so the significance of the linear relationship is interpreted cautiously. Above a Bowen ratio of four, the data largely come from the subtropics.

The regression curve for net surface SW radiation (Fig. 7d) shows greater SW radiation roughly linearly associated with greater DTR except at SW values greater than ~275 W m^{-2} where the relationship flattens out. This is consistent with the regression curve for downward TOA SW radiation (Fig. 6b).

The regression curves for net surface LW radiation, surface sensible heat flux, and net surface SW radiation have broadly linear relationships with DTR. As these energy budget terms are expressed in the same units, the slope of a linear regression between monthly mean DTR and each of these SEB terms provides a measure of the relative importance of these parameters (Table 6). DTR exhibits significantly greater variation with net surface LW radiation than it does with changes in surface sensible heat or net surface SW radiation.

The surface energy balancing term represents the effects of ground fluxes, changes in ground heat capacity, vertical or horizontal heat transport, and anomalies due to inaccuracies in ERA-40 flux calculations. The regression curve (Fig. 7e) shows both positive and negative values (up to 100 W m^{-2}) associated with smaller values of DTR.

The regression curve for latent heat flux (Fig. 7f) suggests greater latent heat flux is associated with smaller DTR over the range of fluxes commonly experienced. The low deviance explained suggests a weak or highly confounded connection. In support of this result, a GAM of DTR against evaporative water flux produced a deviance explained of only 1.4%.

The strong relationship between DTR and net LW radiation was analyzed using linear regression applied to the 12 monthly values of DTR and net LW radiation for each separate grid cell. The R^2 values for the regressions were skewed toward 1 with a median value of 71.2%. The fit of the linear regression for net LW radiation was better than for the other surface energy budget terms

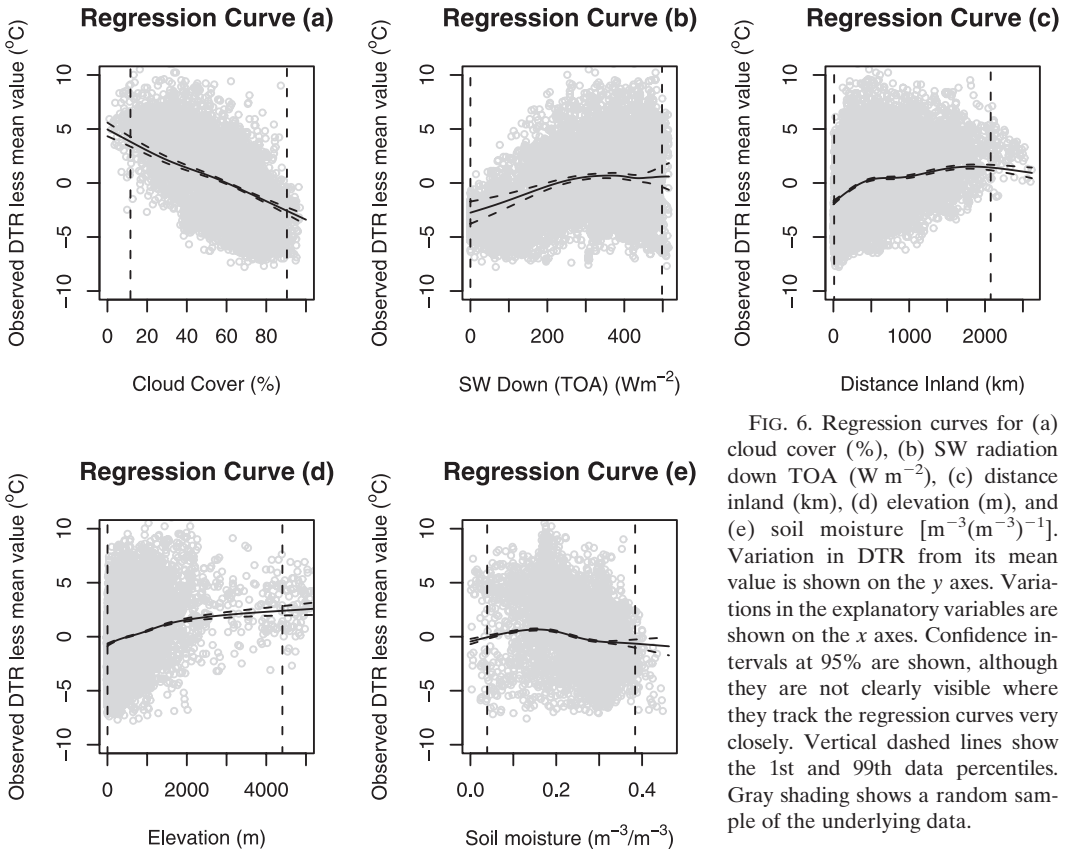

FIG. 6. Regression curves for (a) cloud cover (%), (b) SW radiation down TOA (W m^{-2}), (c) distance inland (km), (d) elevation (m), and (e) soil moisture [$m^{-3}(m^{-3})^{-1}$]. Variation in DTR from its mean value is shown on the *y* axes. Variations in the explanatory variables are shown on the *x* axes. Confidence intervals at 95% are shown, although they are not clearly visible where they track the regression curves very closely. Vertical dashed lines show the 1st and 99th data percentiles. Gray shading shows a random sample of the underlying data.

where the median R^2 values were 45.2%, 42.9%, 38.6%, 32.7%, and 29.9% for sensible heat, net SW radiation, LW radiation down, latent heat, and LW radiation up, respectively.

The geographic pattern of correlation between the 12 monthly values of DTR and net LW radiation (Fig. 8) shows that highest correlations were located in moist tropical regions. Regions with the weakest correlations were located along the coasts and at high latitudes. The driving influence of solar radiation is reflected in the zonal pattern of the correlations, although there are clear regional departures. Some of the factors responsible for geographic variations in the correlation between DTR and net LW radiation are shown in Fig. 9. Grid cells with high correlations between DTR and net LW radiation have greater TOA SW radiation, higher mean maximum and minimum temperatures, greater precipitation, and greater humidity. These factors all contribute to greater fluxes of latent heat, LW radiation up and LW radiation down. The linear regression of DTR and net LW radiation had a mean slope of -0.19 ± 0.05 K $(W\ m^{-2})^{-1}$ averaged over all grid cells. Variations in the slope between grid cells were most closely related to variations in annual mean cloud cover and soil moisture, with correlations of -0.52 and -0.57, respectively.

The variations in linear regression between DTR and net LW radiation were investigated by selecting a number of cells as case studies (Fig. 10). The grid cell located at 19.75°N, 94.75°E had R^2 of 99.0% and slope of -0.13 ± 0.004 K $(W\ m^{-2})^{-1}$. This cell had monthly changes that were almost linear, with DTR increasing from a minimum in June–August to a maximum in January–March. This is a monsoonal location in Southeast Asia approximately 150 km inland. Typical of regions where the correlation of DTR and net LW radiation was strong, it had high specific humidity, high annual mean precipitation, high maximum and minimum temperatures, and was located away from the coast.

TABLE 4. Deviance explained by separate GAM regression models between DTR and cloud cover at 3 different heights. DTR data are from CRU TS 2.1 and includes monthly mean data for all months and vegetation groups. The variation in DTR is the variation of monthly mean CRU gridcell values from the global annual mean DTR. Cloud cover is from ERA-40 reanalysis data.

Cloud cover level	Deviance explained (%)
Low	50.2
Medium	22.5
High	20.7

TABLE 5. Deviance explained by GAM models between monthly mean DTR (response) and the surface energy budget terms. The variation in DTR is the variation of monthly mean CRU gridcell values from the global annual mean DTR. The results are described in section 4d.

Surface radiation and heat fluxes	Deviance explained (%)
Net LW radiation	57.3
Sensible heat	40.2
Bowen ratio	37.2
Net SW radiation	27.3
LW radiation down	15.7
Balancing term	14.5
LW radiation up	14.3
Latent heat	2.9

The grid cell located at 68.25°N, 133.75°E had lower R^2 (71.6%) and a slope of -0.30 ± 0.06 K (W m^{-2})$^{-1}$. The relationship followed linear trajectories from January to March and from August to January, driven by changing net solar radiation. Breaks in this pattern were found to be associated with the thawing and freezing of surface moisture and snow. The reduction in DTR from April to May coincides with the transition of maximum temperatures from below to above freezing point. The increase in DTR from May to June coincides with the transition of minimum temperatures from below to above freezing.

The grid cell located at 62.75°N, 66.25°W on a peninsula approximately 50 km from the coast had R^2 of 5.2% and a regression slope of -0.02 ± 0.02 K (W m^{-2})$^{-1}$. Changes in wind direction between continental northeasterly winds and oceanic southwesterly winds, seasonal changes in the surface albedo from over 0.60 in spring to less than 0.15 in summer, and the freezing/thawing of surface moisture and snow are likely to have disrupted any linear relationship. DTR also varied over a narrow range of values typical of many coastal locations.

Net LW radiation was strongly correlated with cloud cover and soil moisture in regions where there was also a strong correlation between net LW radiation and DTR. Where the correlation coefficient between net LW radiation and DTR was less than -0.98, the correlation coefficient between cloud cover and net LW radiation was 0.94 and between soil moisture and net LW radiation it was 0.95. These results point to cloud cover and soil moisture exerting an influence on DTR through changes in upward and downward surface LW radiation.

5. Discussion and conclusions

The near linear relationship between DTR and net surface LW radiation (Fig. 7a) is consistent with results using ERA-40 data for the Madeira River basin in the Amazon (Betts 2004). High correlations of cloud cover, soil moisture, and precipitation with net surface LW radiation are in agreement with the conclusions of Dai et al. (1999) that clouds combined with secondary effects from soil moisture and precipitation exert a strong influence on DTR. Our results, however, show that the effect of clouds on DTR is more clearly described by changes in net LW radiation rather than by changes in surface solar radiation.

Net LW radiation explained 62% of the variation in monthly mean DTR observed over global land (excluding Greenland and Antarctica). Greater net LW fluxes away from the surface were associated with larger DTR values except for net fluxes more negative than -100 W m^{-2} where the relationship with DTR weakened. Linear regression of the 12 monthly values for each separate grid cell demonstrated that the relationship between DTR and net LW radiation was robust throughout the annual cycle. The median deviance explained was 71.2% increasing to over 95% in moist tropical regions.

The linear relationship between DTR and surface net LW radiation varied geographically. It was strongest in tropical locations that had high maximum and minimum temperatures, high specific humidity and precipitation, and that were located inland. An active hydrological cycle with relatively high surface latent heat fluxes appears to define these locations. Away from the tropics divergences from linearity in the DTR–net LW relationship were caused by soil moisture freezing–thawing and advection. The importance of this has previously been illustrated by Viterbo et al. (1999) in the context of modeling stable boundary layers. Schwartz (1996) concluded that, in addition to the loss of snow cover contributing to the discontinuity in DTR trends in midlatitude regions during Northern Hemisphere spring, more frequent southerly winds and increased cloud ceiling heights could also be contributory factors. While our regression analysis did not rank highly the influence of wind speed or wind direction on DTR, these variables could still have played a minor role within the results and changes in cloud height were not investigated in our analysis. Betts (2004) found the slope of the linear regression between DTR and net surface LW radiation decreased by approximately 20% on moving from the tropics to higher latitudes. We did not find a clear trend between the slope and latitude but found variation in the slope to be most closely related to annual mean cloud cover and soil moisture. Further detailed observations and/or modeling calculations would be necessary to provide deeper insight.

The GAM regression model found DTR to have a strong relationship with vegetation type. Removing vegetation groups from GAM_{dtr} reduced deviance explained

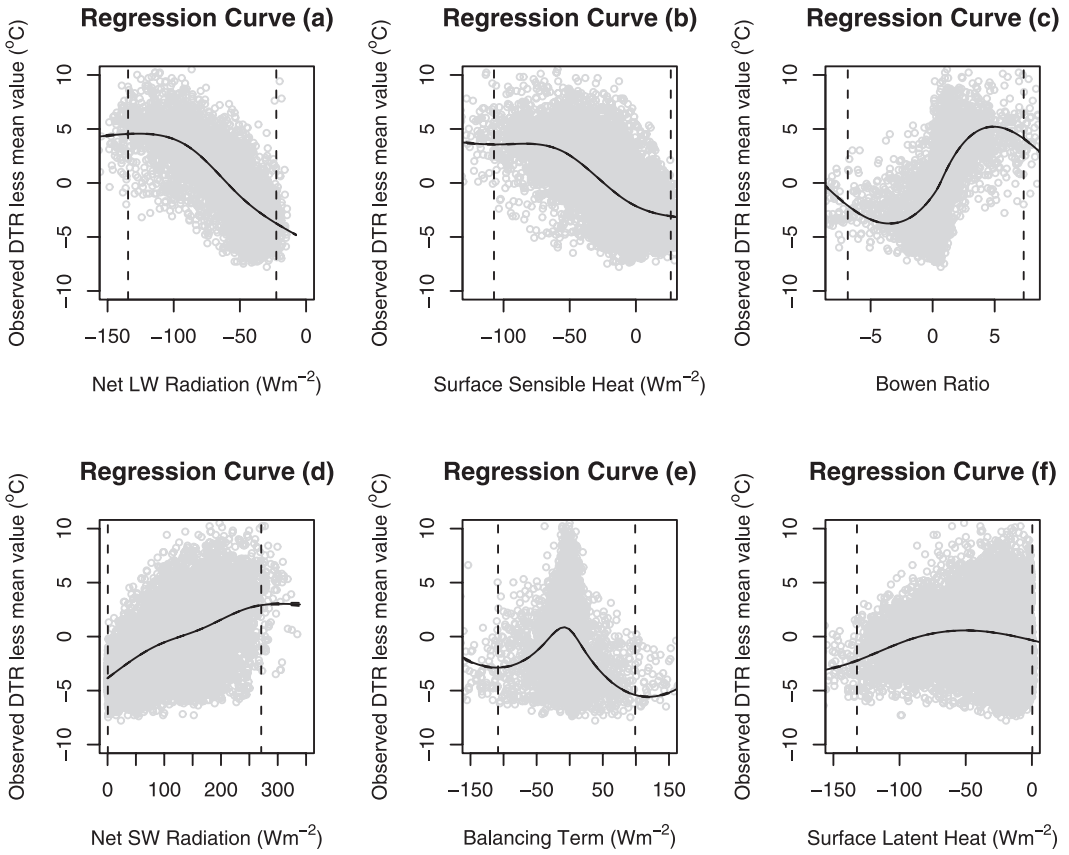

FIG. 7. Regression curves for (a) net surface LW radiation, (b) surface sensible heat flux, (c) Bowen ratio, (d) net surface SW radiation, (e) energy budget balancing term, and (f) surface latent heat flux. Variation in DTR from its mean value is shown on the *y* axes. Energy fluxes are shown on the *x* axes with positive values representing fluxes input to the surface and negative values fluxes away from the surface. Confidence intervals at 95% are shown, although they are not clearly visible where they track the regression curves very closely. Vertical dashed lines show the 1st and 99th data percentiles. Gray shading shows a random sample of the underlying data.

by 6.5% compared with 5.1% when cloud cover was removed. While close coupling of vegetation and climate means that the physical effects of vegetation cannot be isolated by regression alone, the strong connection with DTR was found even after allowing for the effects of key climatic parameters such as cloud cover and solar radiation. The likelihood of a strong relationship between vegetation and DTR is also widely supported in current literature. For example, irrigation of cropland has been found to reduce maximum temperatures (Mahmood et al. 2006; Sen Roy et al. 2007), net SW radiation is influenced by surface albedo (Myhre and Myhre 2003), nighttime temperatures are increased by reduced vegetation and lower soil emissivity in the Sahel region of Africa (Zhou et al. 2007), differences in vegetation cover influence the daytime latent heat flux and nighttime stability (Collatz et al. 2000), differences in the diurnal cycle of biomass heat and biochemical energy storage by different vegetation types affects DTR (Gu et al. 2007), and urbanization reduces DTR (Gallo et al. 1996; Kalnay and Cai 2003). A modeling study of the role of plant physiology in the diurnal and seasonal progression of DTR, especially its impact on surface albedo and moisture fluxes, could clarify the physical contribution from plants. Use of more detailed vegetation classifications could improve diagnosis of the role of vegetation in DTR.

TABLE 6. Slope and R^2 for separate linear regression models between DTR (response variable) against each surface energy budget term using data for all months and vegetation groups.

	R^2 (%)	Slope [K (W m^{-2})$^{-1}$]
Net LW radiation	92.8	$-0.16 \pm 5.2 \times 10^{-5}$
Net SW radiation	84.2	$+0.07 \pm 3.5 \times 10^{-5}$
Sensible heat flux	56.2	$-0.04 \pm 3.8 \times 10^{-5}$
LW radiation up	91.7	$-0.03 \pm 9.8 \times 10^{-6}$
LW radiation down	88.4	$+0.03 \pm 1.4 \times 10^{-5}$

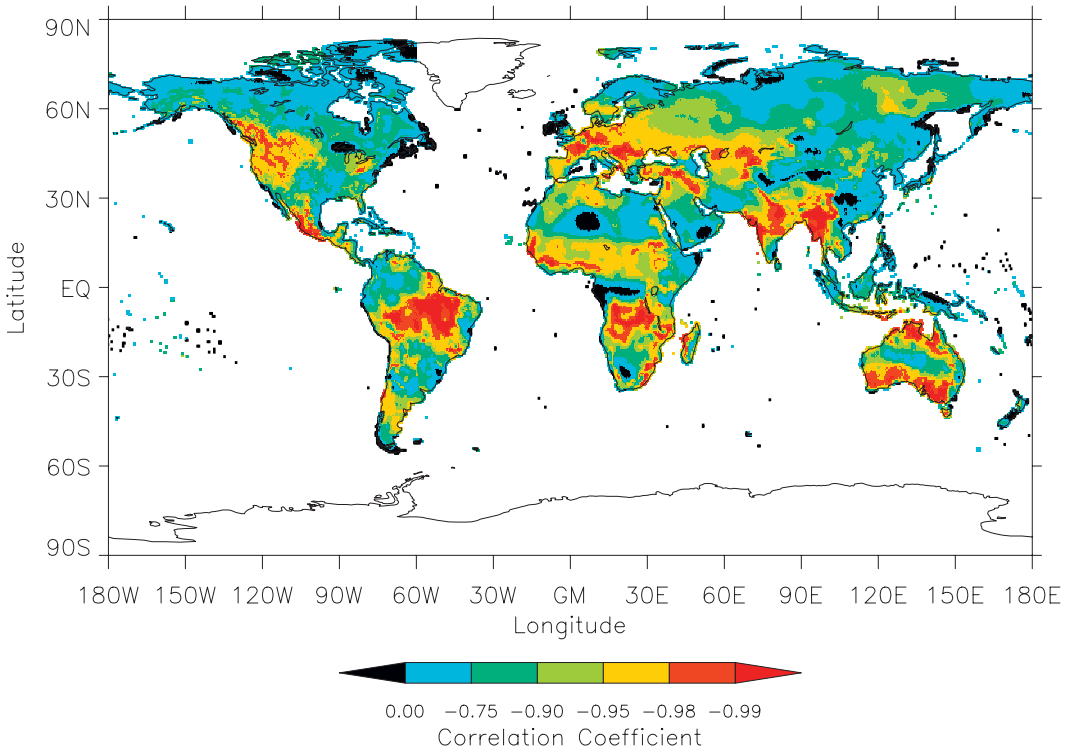

FIG. 8. Geographic pattern of the correlation coefficient between DTR and net LW radiation calculated using the 12 monthly values for each grid cell.

The diurnal cycle of solar radiation drives DTR, and increased insolation is associated with larger DTR values (Rebetez and Beniston 1998). Greater cloud cover and soil moisture are associated with smaller DTR values (Dai et al. 1999), and low-level clouds are more influential for DTR than medium- or high-level clouds (Karl et al. 1993; Geerts 2003; Dai et al. 1999). Up to 150 km, distance inland shows the ameliorating effects of sea breezes on DTR in coastal regions (which cool daytime temperatures) and also the influence of cloud cover changes (Geerts 2003). The increase in DTR with increasing distance inland beyond 150 km, while statistically significant, is not explainable in terms of local meteorology or geography. Higher elevation was associated with greater DTR and is consistent with the multiple linear regression DTR model of Linacre (1992). While this conclusion is valid on a global scale, local terrain, land–sea breezes, and atmospheric circulation could be influential and would dominate on smaller geographic scales. This was demonstrated by Geerts (2003) who identified places where DTR increased with elevation (e.g., western United States 1.9°C km^{-1} in July) and also areas where DTR reduced with elevation (e.g., parts of the Alps 2.1°C km^{-1}).

GAM_{dtr} identified cloud cover, soil moisture, distance inland, downward TOA SW radiation, and elevation as important in the geographic and seasonal variation in DTR. These results supplement the earlier findings discussed above by quantifying and ranking the sensitivity of DTR to each parameter. To provide a more complete description of the geographic and seasonal variation in DTR, the regression models would need to include factors that cause step changes in the monthly progression of DTR, for example, soil moisture freezing, snowmelt/accumulation, and advection of heat and moisture by the atmosphere.

Variations in DTR left unexplained by GAM_{dtr} (20.3%) reflect both random variation and uncertainty in the results. If regression curves are overfitted, random variation would be confounded with model predictions, although there was no clear evidence of this in the predictions of GAM_{dtr}. Uncertainty could arise from the influence of meteorological and surface parameters not considered in this research. Relationships between explanatory variables were not explicitly modeled, as they can be difficult to interpret and computationally expensive. Nevertheless, they could be a further source of uncertainty in these results. Measurement errors in temperature readings are a source of variation in DTR observations that the GAM_{dtr} predictions do not represent. Data quality procedures applied in the preparation of CRU TS 2.1 should help to minimize this error.

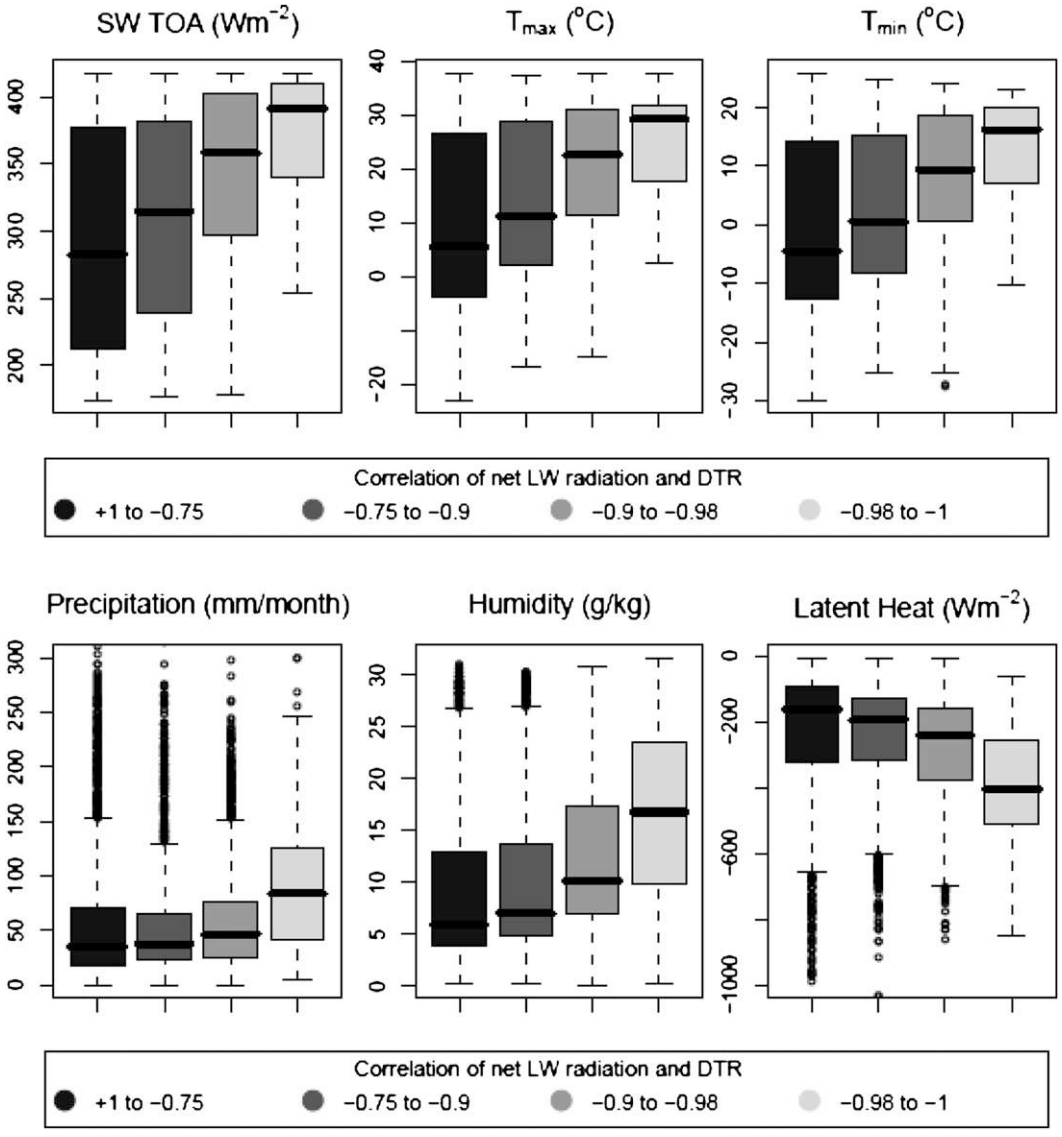

FIG. 9. Annual mean values for SW TOA, maximum temperature (T_{max}), minimum temperature (T_{min}), precipitation, humidity, and surface latent heat flux calculated for each separate grid cell. The median is shown by the bold bar, first and third quartiles by the boundaries of the shaded box, and data outliers by individual points. The annual mean values have been grouped according to the value of the correlation coefficient between net LW radiation and DTR for each grid cell.

Combining data from ERA-40 and CRU TS 2.1 may have increased the uncertainty in our analyses. There were gaps in the completeness of some ERA-40 data fields (e.g., soil moisture). These cells were ignored in the regression calculations. Limitations in the physical parameterization of the ECMWF model used for ERA-40 will have introduced bias in the reanalysis data (Betts et al. 2006). Bias in CRU TS 2.1 is likely to be enhanced for grid cells based on a limited number of underlying observations (e.g., Sahara Desert). CRU TS 2.1 data were at a resolution of 0.5° × 0.5°, but ERA-40 and satellite data were at a coarser resolution. While ERA-40 data were available at 1° × 1° resolution, the coarser resolution was favored because a longer time series of data was available at 2.5° × 2.5° and this resolution was considered suitable for analysis of global-scale influences on DTR.

The modeled data were autocorrelated both spatially and between months. For DTR predictions, this was implicitly captured in the model fitting process. The p values used to assess the statistical significance of regression curves were inflated and the statistical significance of GAM results overstated. This was allowed for

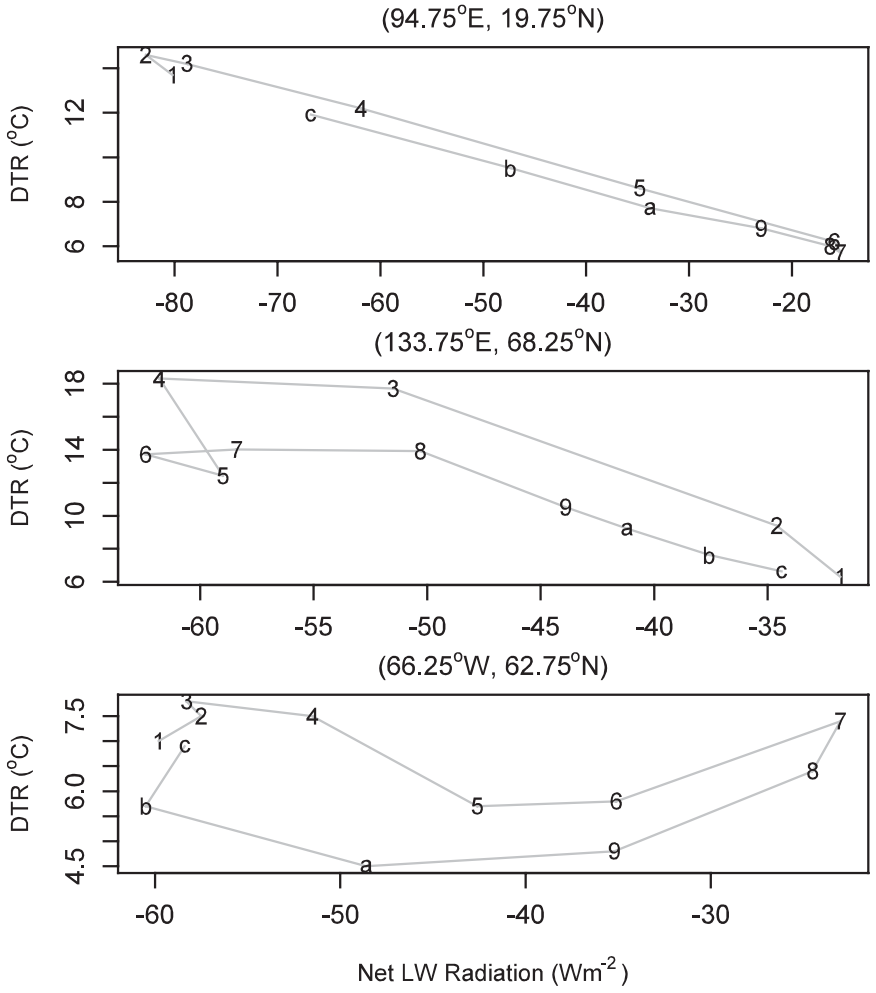

FIG. 10. Monthly mean values of net longwave radiation (*x* axis) plotted against DTR (*y* axis) for three locations with longitude and latitude shown above each plot. The months are represented by 1–9 and a–c for January–December.

in part by the use of 0.1% significance level and was not regarded as a major drawback as the focus was on using regression curves to interpret the relationships with DTR.

Future application of this GAM methodology on regional scales using bespoke explanatory variables could enhance understanding of more localized influences on DTR. Sensitivity to vegetation and cloud cover may be particularly relevant to investigations of the causes of the global downward trend in DTR in the second half of the twentieth century. As identifying cause and effect in regression analysis is difficult, climate modeling could be used to investigate the physical processes underpinning the close relationships of DTR with surface net LW radiation and vegetation.

Acknowledgments. We acknowledge the contributions made by Alan Betts and two anonymous reviewers for helping improve this manuscript. We thank the R software development team and also the British Atmospheric Data Centre for providing access to ECMWF data. Data on aerosol optical depth and solar radiation (TOA) were obtained from the NASA Langley Research Center Atmospheric Science Data Center. We gratefully acknowledge the Natural Environment Research Council for funding the Ph.D. studentship of Lawrence Jackson.

REFERENCES

Bäumer, D., R. Rinke, and B. Vogel, 2008: Weekly periodicities of aerosol optical thickness over central Europe—Evidence of anthropogenic direct aerosol effect. *Atmos. Chem. Phys.,* **8,** 83–90.

Betts, A. K., 2004: Understanding hydrometeorology using global models. *Bull. Amer. Meteor. Soc.,* **85,** 1673–1688.

——, M. Zhao, P. A. Dirmeyer, and A. C. M. Beljaars, 2006: Comparison of ERA40 and NCEP/DOE near-surface datasets

with other ISLSCP-II datasets. *J. Geophys. Res.,* **111,** D22S04, doi:10.1029/2006JD007174.

Bowen, I. S., 1926: The ratio of heat losses by conduction and by evaporation from any water surface. *Phys. Rev.,* **26,** 779–787.

Camillo, P. J., and R. J. Gurney, 1986: A resistance parameter for bare-soil evaporation models. *Soil Sci.,* **141,** 95–105.

Carslaw, D. C., and N. Carslaw, 2007: Detecting and characterising small changes in urban nitrogen dioxide concentrations. *Atmos. Environ.,* **41,** 4723–4733.

Collatz, G. J., L. Bounoua, S. O. Los, D. A. Randall, I. Y. Fung, and P. J. Sellers, 2000: A mechanism for the influence of vegetation on the response of the diurnal temperature range to changing climate. *Geophys. Res. Lett.,* **27,** 3381–3384.

Dai, A., A. D. Del Genio, and I. Y. Fung, 1997: Clouds, precipitation and temperature range. *Nature,* **386,** 665–666.

——, K. E. Trenberth, and T. R. Karl, 1999: Effects of clouds, soil moisture, precipitation and water vapor on diurnal temperature range. *J. Climate,* **12,** 2451–2473.

Darnell, W. L., W. F. Staylor, S. K. Gupta, N. A. Ritchey, and A. C. Wilber, 1992: Seasonal variation of surface radiation budget derived from International Satellite Cloud Climatology Project C1 data. *J. Geophys. Res.,* **97** (D14), 15 741–15 760.

Diner, D. J., and Coauthors, 1998: Multi-angle Imaging SpectroRadiometer (MISR) description and experiment overview. *IEEE Trans. Geosci. Remote Sens.,* **36,** 1072–1087.

Eastman, J. L., M. B. Coughenour, and R. A. Pielke, 2001: The regional effects of CO_2 and landscape change using a coupled plant and meteorological model. *Global Change Biol.,* **7,** 797–815.

Forster, P. M. de F., and S. Soloman, 2003: Observations of a weekend effect in diurnal temperature range. *Proc. Natl. Acad. Sci. USA,* **100,** 11 225–11 230.

Gallo, K. P., D. R. Easterling, and T. C. Peterson, 1996: The influence of land use/land cover on climatological values of the diurnal temperature range. *J. Climate,* **9,** 2941–2944.

Geerts, B., 2003: Empirical estimation of the monthly-mean daily temperature range. *Theor. Appl. Climatol.,* **74,** 145–165.

Gong, D.-Y., D. Guo, and C.-H. Ho, 2006: Weekend effect in diurnal temperature range in China: Opposite signals between winter and summer. *J. Geophys. Res.,* **111,** D18113, doi:10.1029/2006JD007068.

Gu, L., and Coauthors, 2007: Influences of biomass heat and biochemical energy storages on the land surface fluxes and radiative temperature. *J. Geophys. Res.,* **112,** D02107, doi:10.1029/2006JD007425.

Hansen, J., M. Sato, and R. Ruedy, 1995: Long-term changes of the diurnal temperature cycle: Implications about mechanisms of global climate change. *Atmos. Res.,* **37,** 175–209.

Hastie, T. J., and R. Tibshirani, 1990: *Generalized Additive Models*. Chapman and Hall, 352 pp.

Kalnay, E., and M. Cai, 2003: Impact of urbanization and land-use change on climate. *Nature,* **423,** 528–531.

Kan, H., 2007: Diurnal temperature range and daily mortality in Shanghai, China. *Environ. Res.,* **103,** 424–431.

Karl, T. R., and Coauthors, 1993: A new perspective on recent global warming: Asymmetric trends of daily maximum and minimum temperature. *Bull. Amer. Meteor. Soc.,* **74,** 1007–1023.

Linacre, E., 1982: The effect of altitude on the daily range of temperature. *Int. J. Climatol.,* **2,** 375–382.

——, 1992: *Climate Data and Resources: A Reference and Guide*. Routledge, 366 pp.

Mahmood, R., S. A. Foster, T. Keeling, K. G. Hubbard, C. Carlson, and R. Leeper, 2006: Impacts of irrigation on 20th Century temperature in the northern Great Plains. *Global Planet. Change,* **54,** 1–18.

Mitchell, T. D., and P. D. Jones, 2005: An improved method of constructing a database of monthly climate observations and associated high-resolution grids. *Int. J. Climatol.,* **25,** 693–712.

Montgomery, D. C., and E. A. Peck, 2006: *Introduction to Linear Regression Analysis*. 4th ed. Wiley/Blackwell, 640 pp.

Murphy, D. M., S. L. Capps, J. S. Daniel, G. J. Frost, and W. H. White, 2008: Weekly patterns of aerosol in the United States. *Atmos. Chem. Phys.,* **8,** 2729–2739.

Myhre, G., and A. Myhre, 2003: Uncertainties in radiative forcing due to surface albedo changes caused by land-use changes. *J. Climate,* **16,** 1511–1524.

Ohmura, A., 1984: On the cause of FRAM type seasonal change in diurnal amplitude of air temperature in polar regions. *Int. J. Climatol.,* **4,** 325–338.

Przybylak, R., 2000: Diurnal temperature range in the arctic and its relation to hemispheric and arctic circulation patterns. *Int. J. Climatol.,* **20,** 231–253.

R Development Core Team, cited 2007: A language and environment for statistical computing. R Foundation for Statistical Computing. [Available online at http://www.R-project.org.]

Rebetez, M., and M. Beniston, 1998: Changes in sunshine duration are correlated with changes in daily temperature range this century: An analysis of Swiss climatological data. *Geophys. Res. Lett.,* **25,** 3611–3613.

Reiss, R., 2006: Temporal trends and weekend-weekday differences for benzene and 1,3-butadiene in Houston, Texas. *Atmos. Environ.,* **40,** 4711–4724.

Schwartz, M. D., 1996: Examining the spring discontinuity in daily temperature ranges. *J. Climate,* **9,** 803–808.

Sen Roy, S., R. Mahmood, D. Niyogi, M. Lei, S. A. Foster, K. G. Hubbard, E. Douglas, and R. Pielke Sr., 2007: Impacts of the agricultural Green Revolution–induced land use changes on air temperatures in India. *J. Geophys. Res.,* **112,** D21108, doi:10.1029/2007JD008834.

Tuomenvirta, H., H. Alexandersson, A. Drebs, P. Frich, and P. O. Nordli, 2000: Trends in Nordic and Arctic temperature extremes and ranges. *J. Climate,* **13,** 977–990.

Uppala, S. M., and Coauthors, 2005: The ERA-40 Re-Analysis. *Quart. J. Roy. Meteor. Soc.,* **131,** 2961–3012.

Viterbo, P., A. Beljaars, J.-F. Mahfouf, and J. Teixeira, 1999: The representation of soil moisture freezing and its impact on the stable boundary layer. *Quart. J. Roy. Meteor. Soc.,* **125,** 2401–2426.

Wild, M., A. Ohmura, and K. Makowski, 2007: Impact of global dimming and brightening on global warming. *Geophys. Res. Lett.,* **34,** L04702, doi:10.1029/2006GL028031.

Wilson, M. F., and A. Henderson-Sellers, 1985: A global archive of land cover and soils data for use in general circulation climate models. *Int. J. Climatol.,* **5,** 119–143.

Wood, S. N., 2006: *Generalized Additive Models: An Introduction with R*. Chapman and Hall/CRC, 416 pp.

Zhou, L., R. E. Dickinson, Y. Tian, R. S. Vose, and Y. Dai, 2007: Impact of vegetation removal and soil aridation on diurnal temperature range in a semiarid region: Application to the Sahel. *Proc. Natl. Acad. Sci. USA,* **104,** 17 937–17 942.

——, A. Dai, Y. Dai, R. S. Vose, C.-Z. Zou, Y. Tian, and H. Chen, 2009: Spatial dependence of diurnal temperature range trends on precipitation from 1950 to 2004. *Climate Dyn.,* **32,** 429–440.